REFERENCES

Berge, Ph., Ribon, C., and Saint Paul, P. (1976) Effect of Hydrogen on the Corrosion Steels in High Temperature Water. Corrosion, 32(6), 223-228.

Cabrera-Sierra, R., García, I., Sosa, E., Oropeza, T., González, I. (2000) Electrochemical Behavior of Carbon Steel in Alkaline Sour Environments measured by Electrochemical Impedance Spectroscopy, Electrochimica Acta, 46, 487-497.

Cheng, Y.F. and Steward, F.R. (2004) Corrosion of Carbon Steels in High Temperature Water Studied by Electrochemical Techniques, Corrosion Science. 46(10), 2405-2420.

Fontana, M.G. (1986) Corrosion Engineering. 3rd ed. Singapore: McGraw- Hill.

Heitz, E. (1995) Mechanistically Based Prevention Strategies of Flow-Induced Corrosion. Electroachimica Acta, 41(4), 503-509.

Jones, D.A. (1992) Principles and Prevention of Corrosion, International ed. Singapore: Maxwell Macmillan.

Kim, Y.J. (1994) Characterization of Oxide Film Formed on Type 316 Stainless Steel in 288 °C Water in Cyclic Normal and Hydrogen Water Chemistries. Corrosion, 51(11), 849-860.

Kim, Y.J. (1996) Analysis of Oxide Film Formed on Type 304 Stainless Steel in 288 °C Water Containing Oxygen, Hydrogen and Hydrogen Peroxide. Corrosion, 55(1), 81-88.

Lang, L.C. (2000) Modeling corrosion for activity transport in CANDU reactors. M.S. Thesis, Faculty of Engineering, University of New Brunswick.

Lister, D.H., Davidson, R.D., and McAlphine, E. (1987) The Mechanism and Kinetics of Corrosion Product Release from Stainless Steel in Lithiated High Temperature Water. Corrosion Science, 27, 113-140.

Lister, D.H., Gautheir, P., Goszczynski, J., and Slade, J. (1998) The Accelerated Corrosion of CANDU Primary Piping. Paper presented at the 1998 JAIF International Conference, Japan Atomic Industrial Forum on Water Chemistry Nuclear Power Plants.

Liter, D.H., Arbeau, N., and Johari, J.M.C. (1994) Erosion and Cavitation in the CANDU Primary Heat Transport System Report. University of New Brunswick.

Potter, E.C. and Mann, G.M.W. (1962) Oxidation of Mild Steel in High Temperature Aqueous Systems. First International Congress on Metallic Corrosion, Butterworth, London.

Robertson, J. (1989) The Mechanism of High Temperature Aqueous Corrosion of Steel. Corrosion science, 29(11/12), 1275-1291.

Sanchez-Caldera, L.E., Griffith, P., and Rabinnowicz, E. (1998) The Mechanism of Corrosion-Erosion in Steam Extraction Lines of Power Stations. Journal of Engineering for Gas Turbines and Power, 110, 180-184.

Silverman, D.C. (1987) Primer on the AC Impedance Technique. Electrochemical Techniques for Corrosion Engineering (R. Baboian, ed), NACE, 73.

Stellwag, B. (1998) The Mechanism of Oxide Film Formation on Austenitic Stainless Steels in High Temperature Water. Corrosion Science, 40(2-3), 337-370.

Supa-Amornkul, S. (2000) Numerical Analysis of Thermalhydraulics for Flow-Assisted Corrosion in CANDU Outlet Feeder Pipes. M.S. Thesis, Faculty of Engineering, University of New Brunswick.

Silpsrikul, O. (2001) Modeling of the Thinning of the CANDU Reactor Feeder Pipes. M.S. Thesis, The Petroleum and Petrochemical College, Chulalongkorn University, Bangkok, Thailand.

Tomlinson, L. (1981) Mechanism of Corrosion of Carbon and Low Alloy Ferritic Steels by High Temperature Water, Corrosion-NACE, 39(10), 591-596.

Tremaine, P.R. and Leblanc, J.C. (1980) The Solubility of Magnetite and the Hydrolysis and Oxidation of Fe^{2+} in water at 300 °C. Journal of Solution Chemistry, 9(6), 415-442.

Uhlig, H.H. and Revie, R.W. (1985) Corrosion and Corrosion control. 3rd ed. Singapore: Wiley.

APPENDICES

Appendix A Scanning Electron Microscope Photographs

A.1 Scanning Electron Microscope Photographs for A106B Carbon Steel

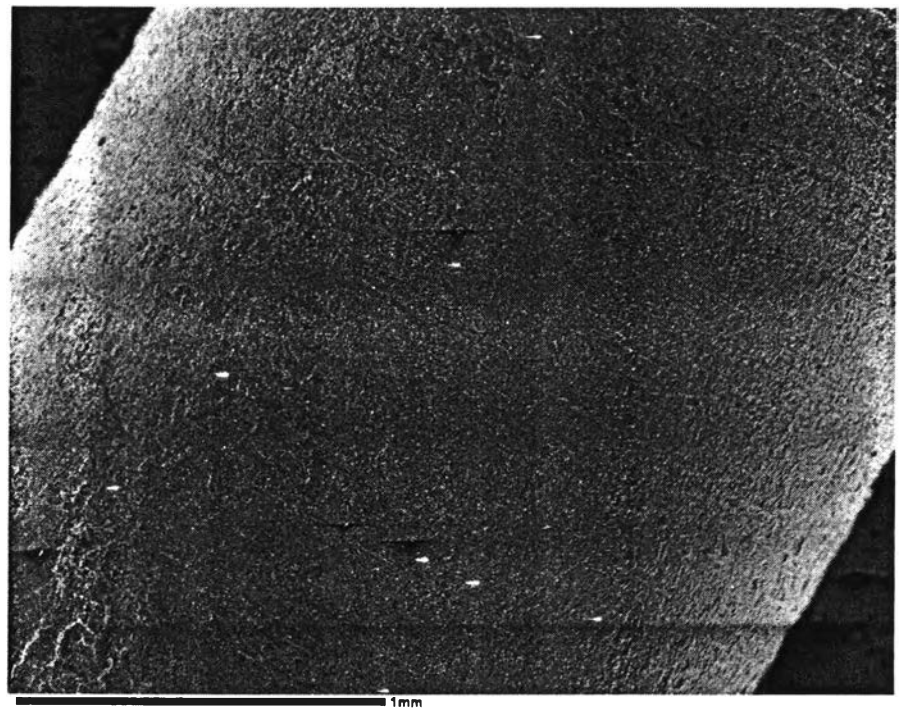

(a) At 50X magnification

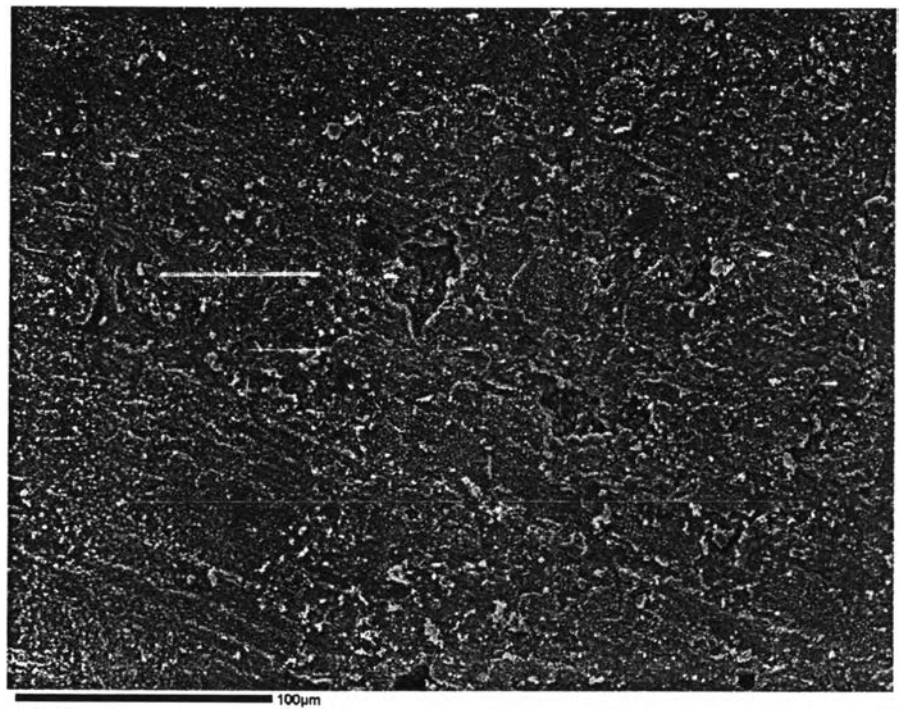

(b) At 350X magnification

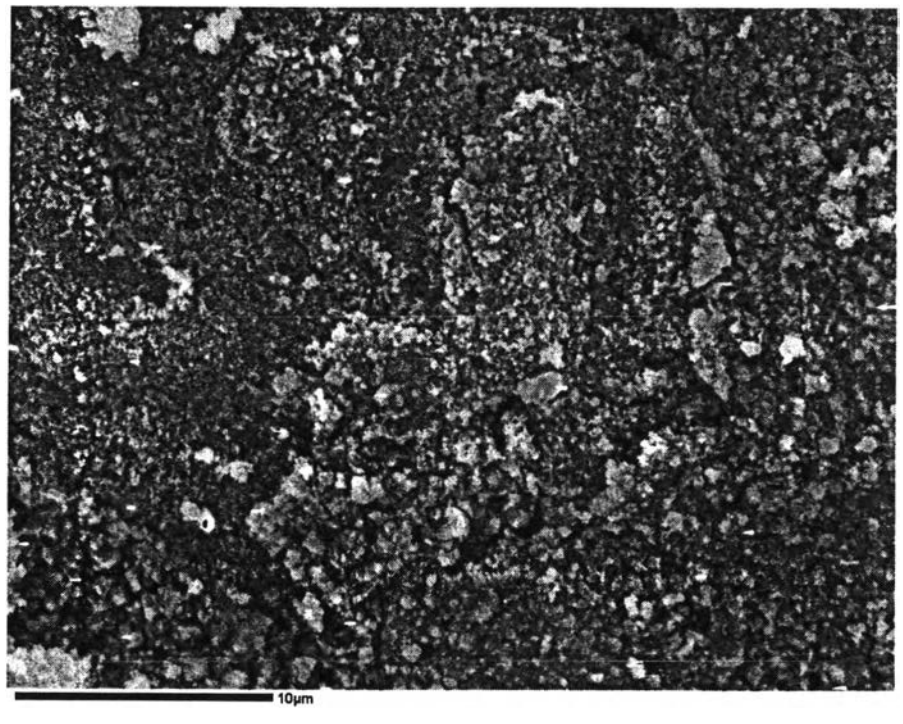

(c) At 3,500X magnification

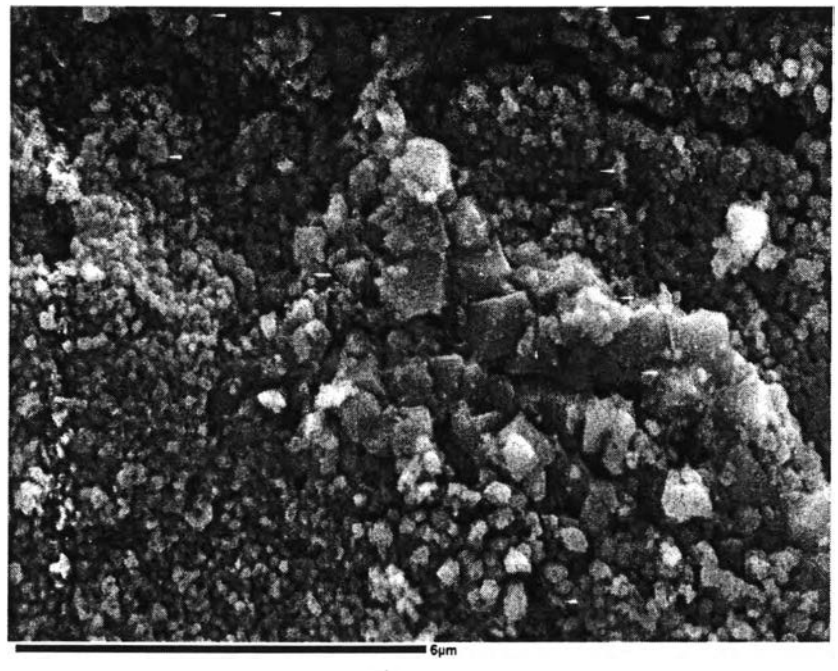

(d) At 10,000X magnification

A.2 Scanning Electron Microscope Photographs for Qinshan Steel

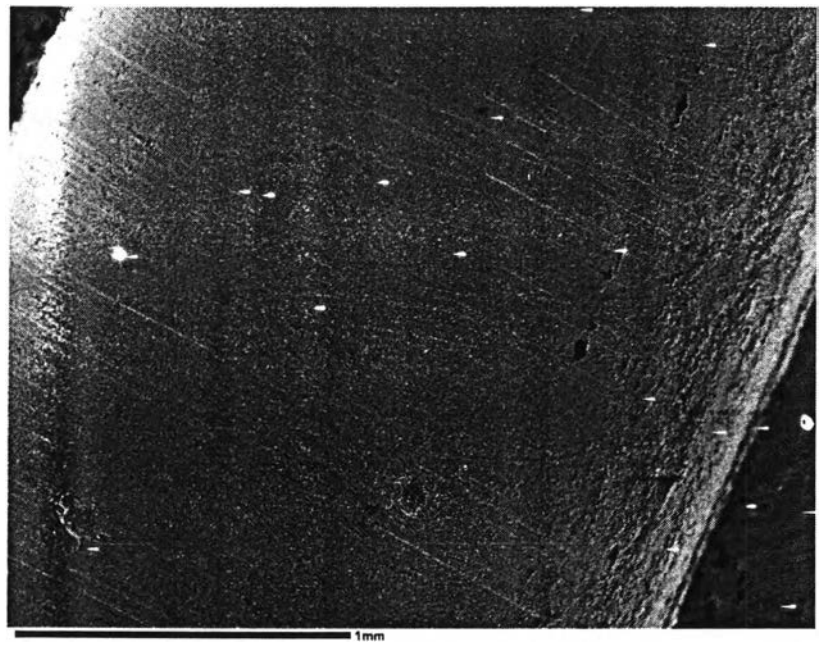

(a) At 50X magnification

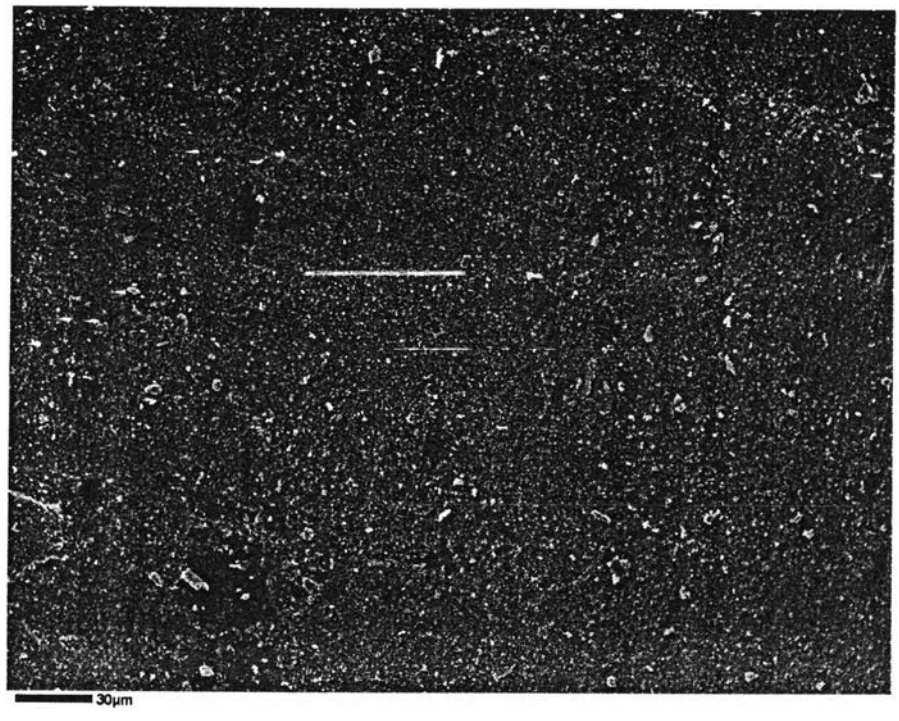

(b) At 350X magnification

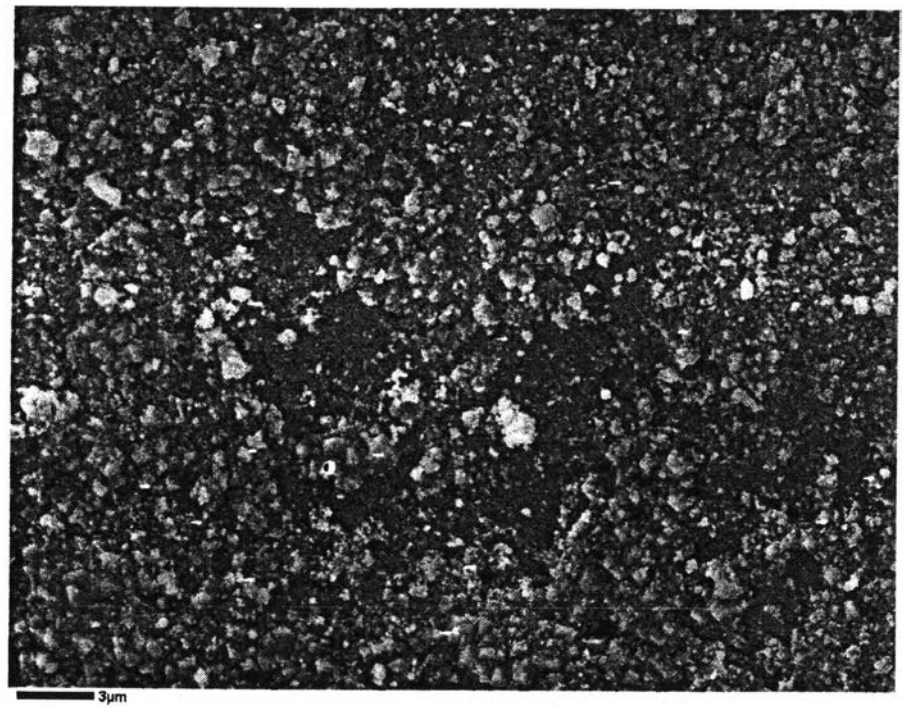

(c) At 3,500X magnification

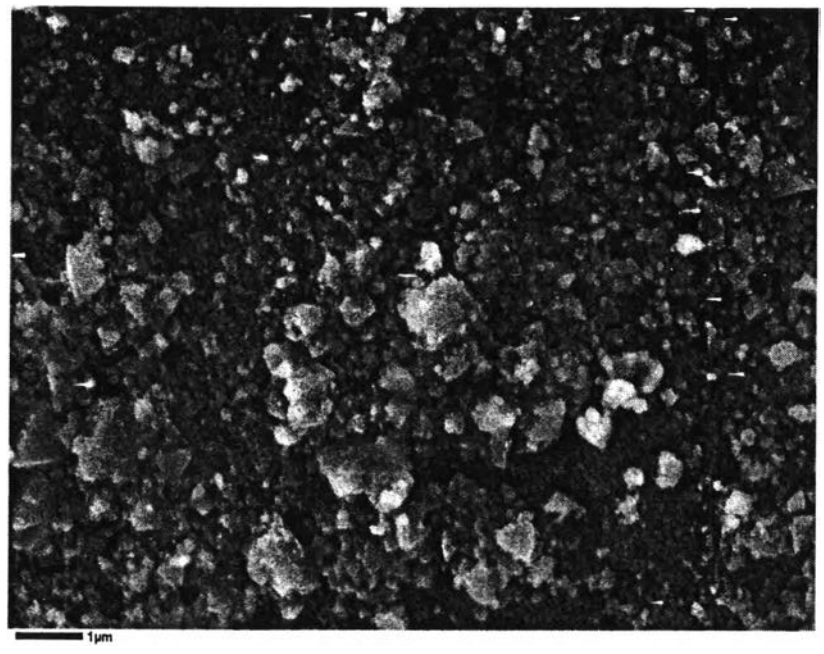

(d) At 10,000X magnification

A.3 Scanning Electron Microscope Photographs for 2.5%Cr/1.0%Mo Steel

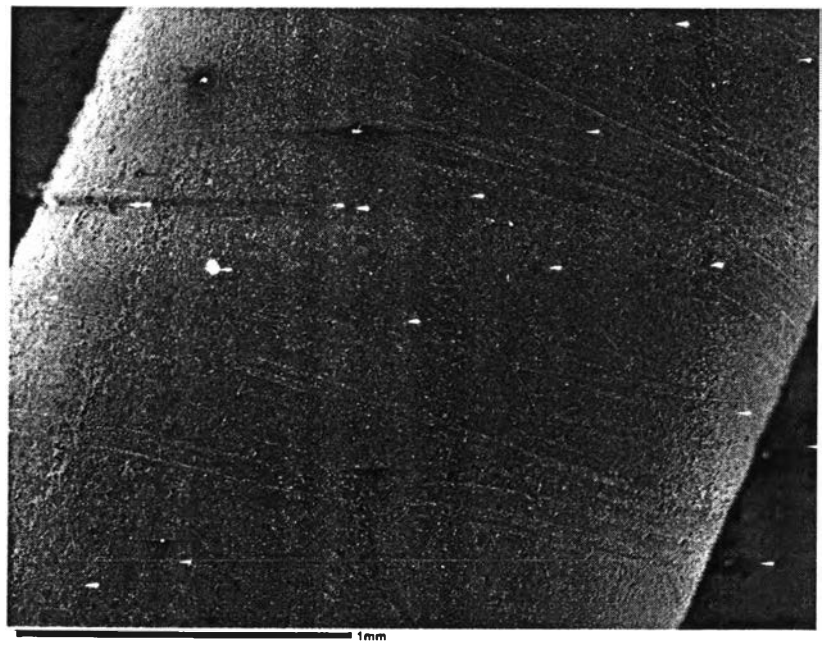

(a) At 50X magnification

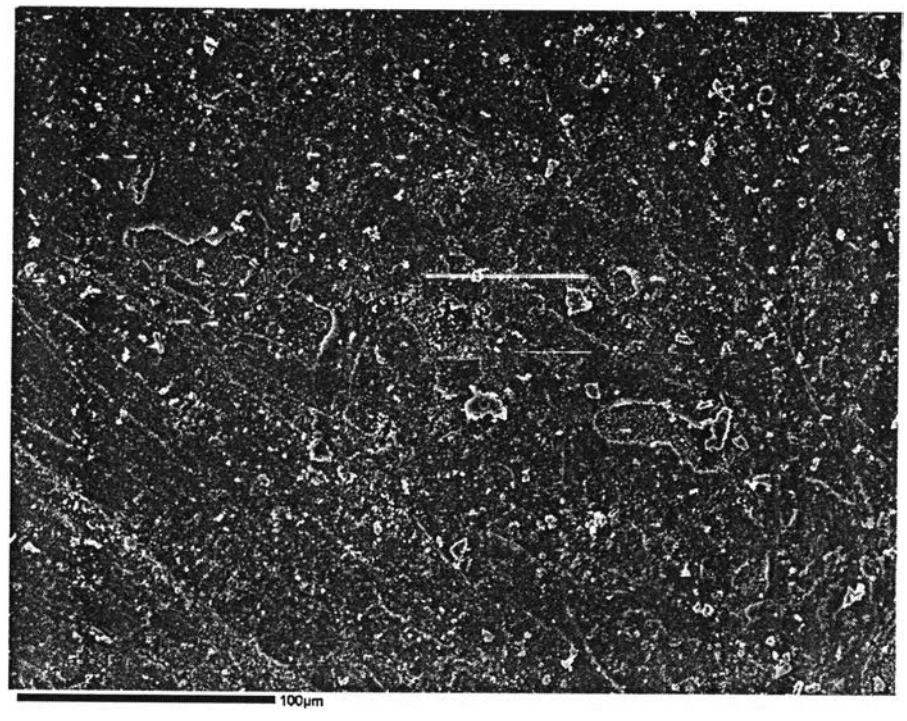

(b) At 350X magnification

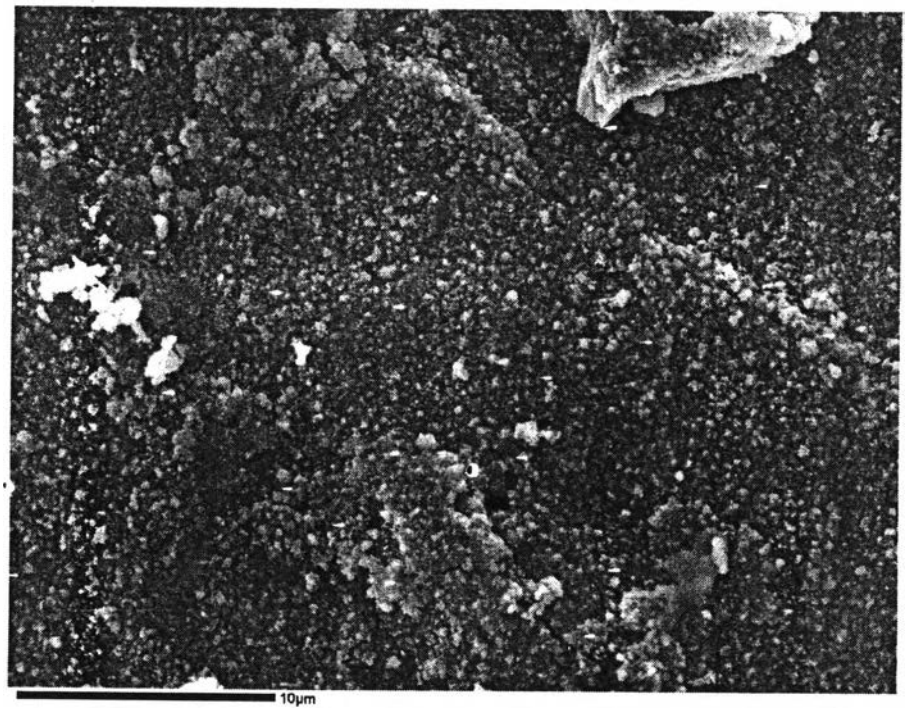

(c) At 3,500X magnification

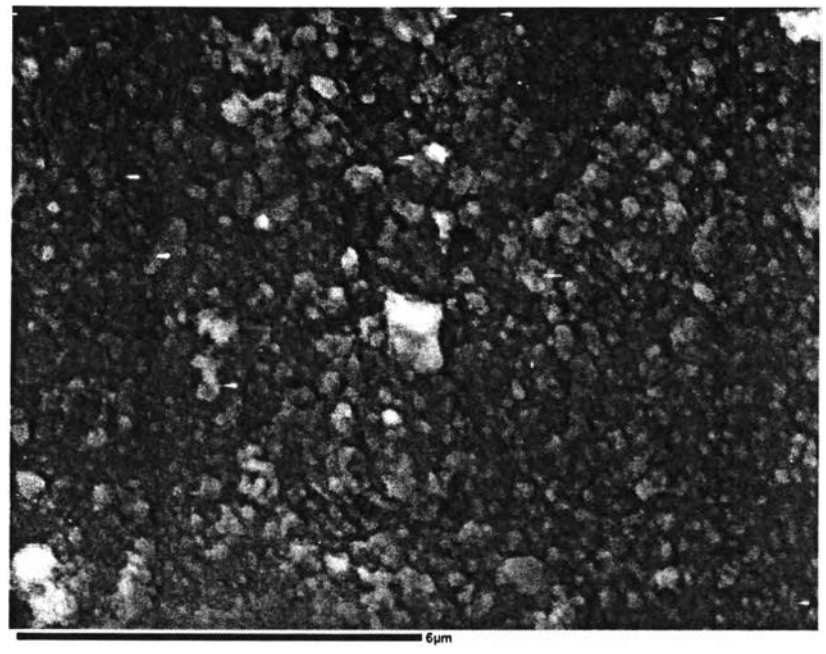

(d) At 10,000X magnification

A.4 Scanning Electron Microscope Photographs for 304 Stainless Steel

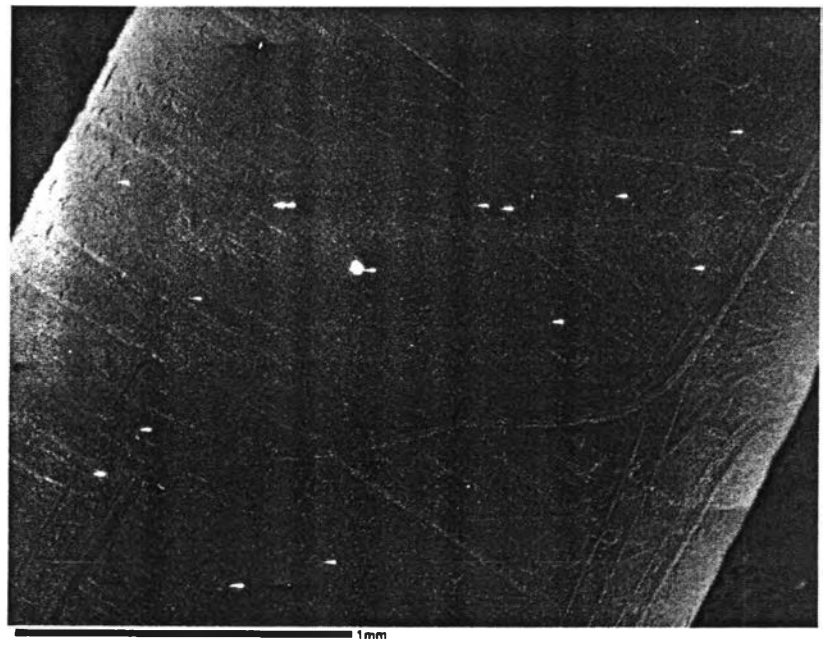

(a) At 50X magnification

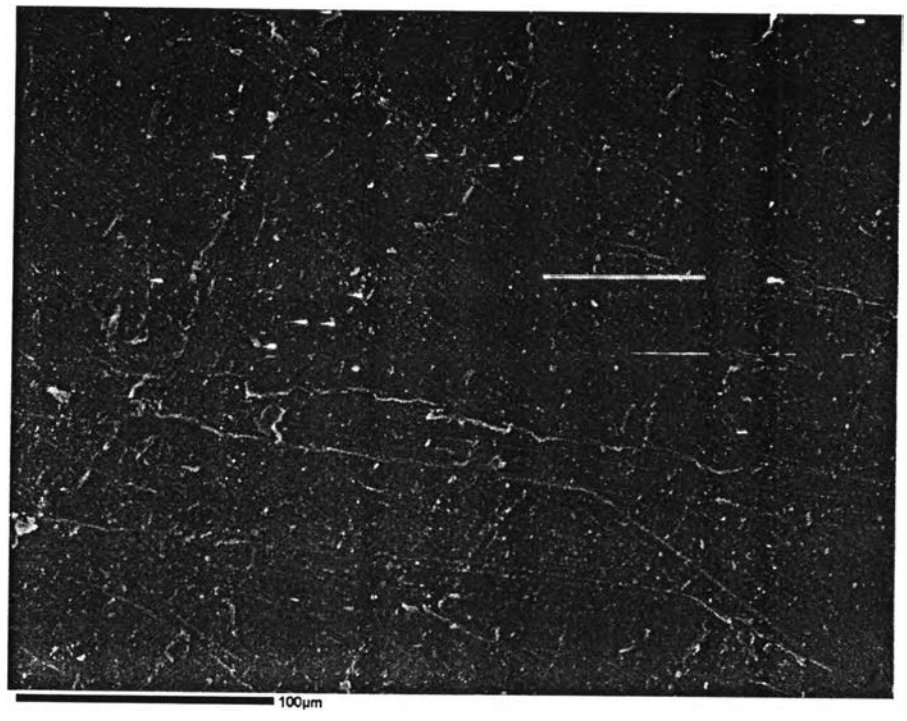

(b) At 350X magnification

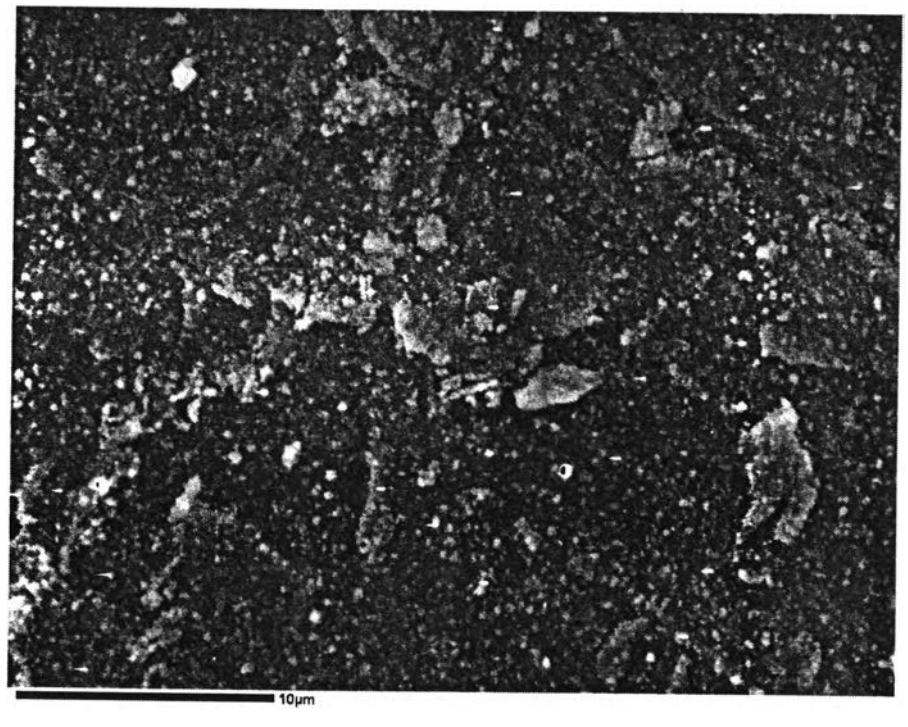

(c) At 3,500X magnification

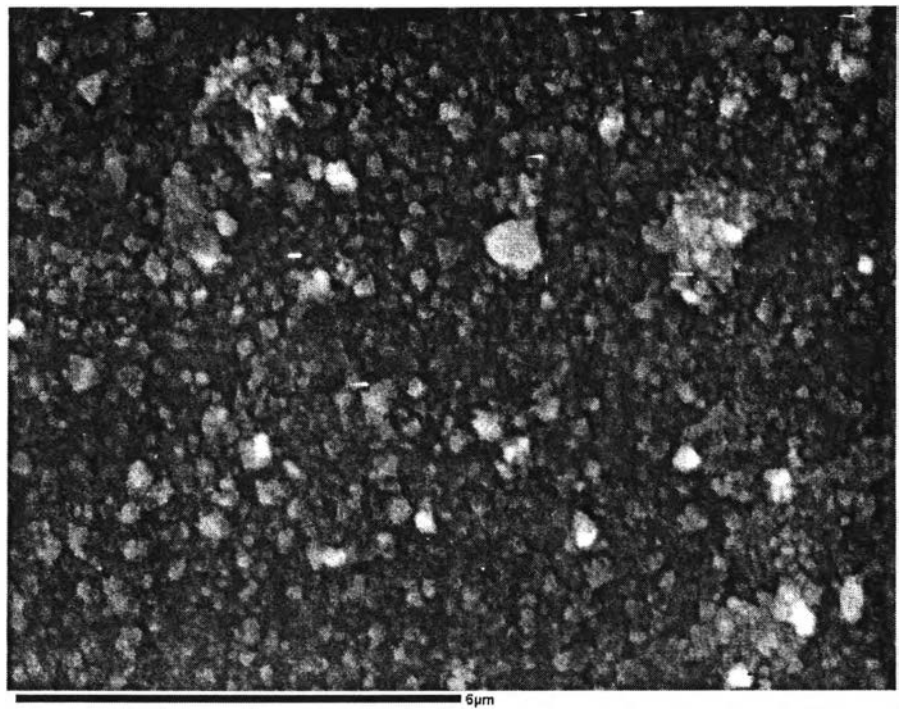

(d) At 10,000X magnification

Appendix B Electron Diffraction Patterns

B.1 Electron Diffraction Patterns for A106B Carbon Steel

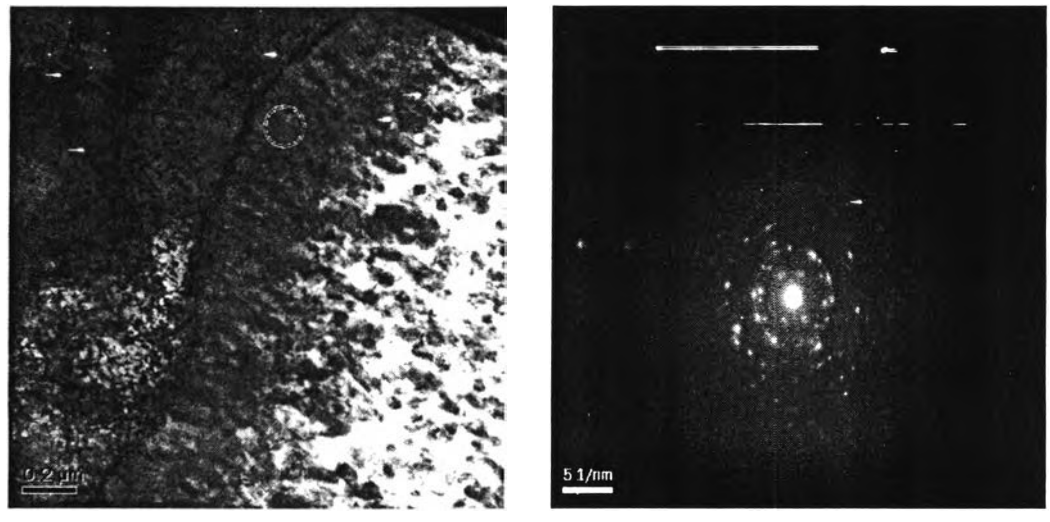

(a) A106B_IN_1

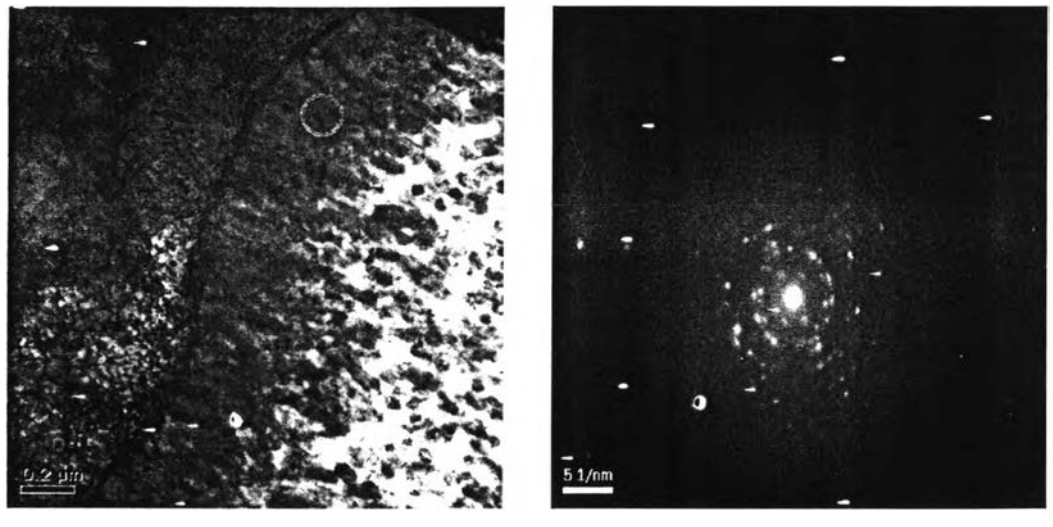

(b) A106B_IN_2

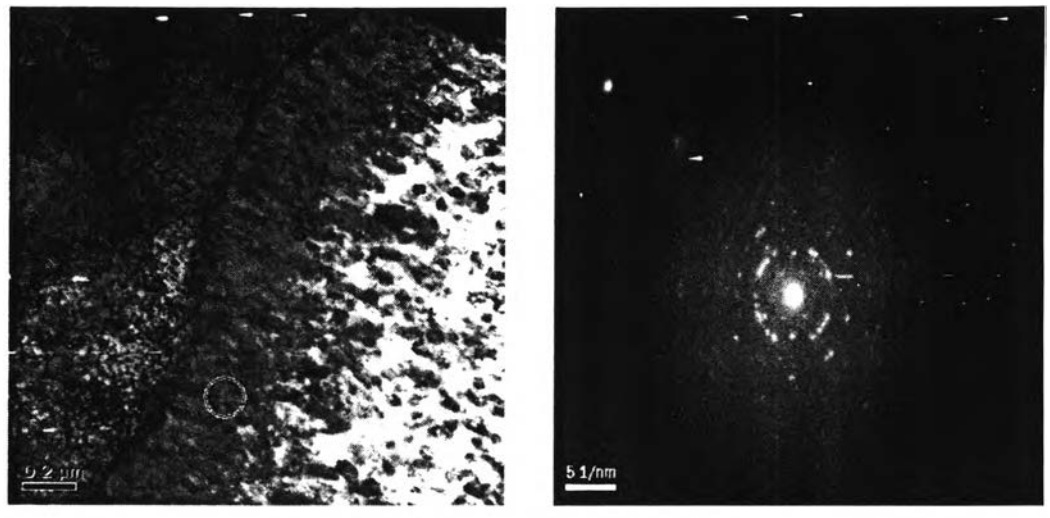

(c) A106B_IN_3

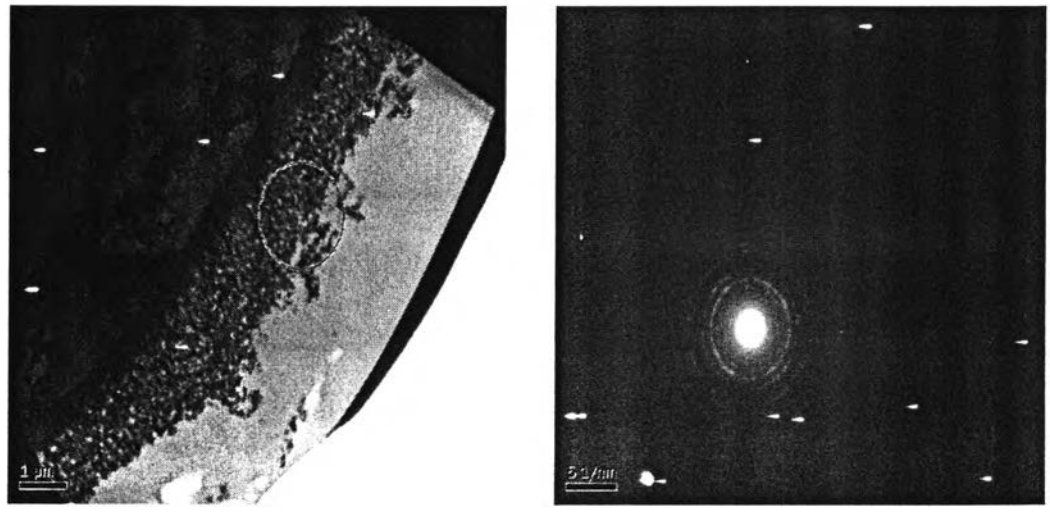

(d) A106B_OUT_1

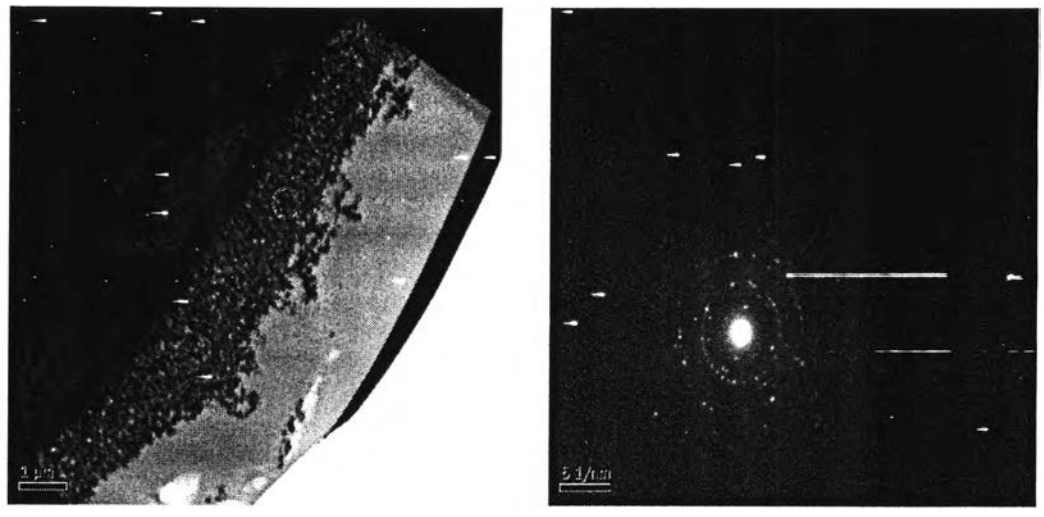

(e) A106B_OUT_2

B.2 Electron Diffraction Patterns for Qinshan Steel

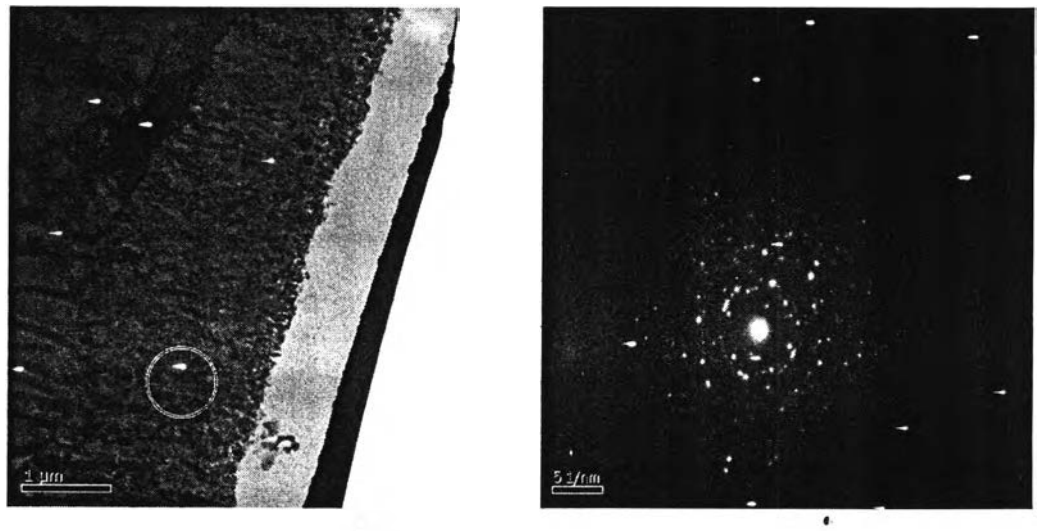

(a) Qinshan_IN_1

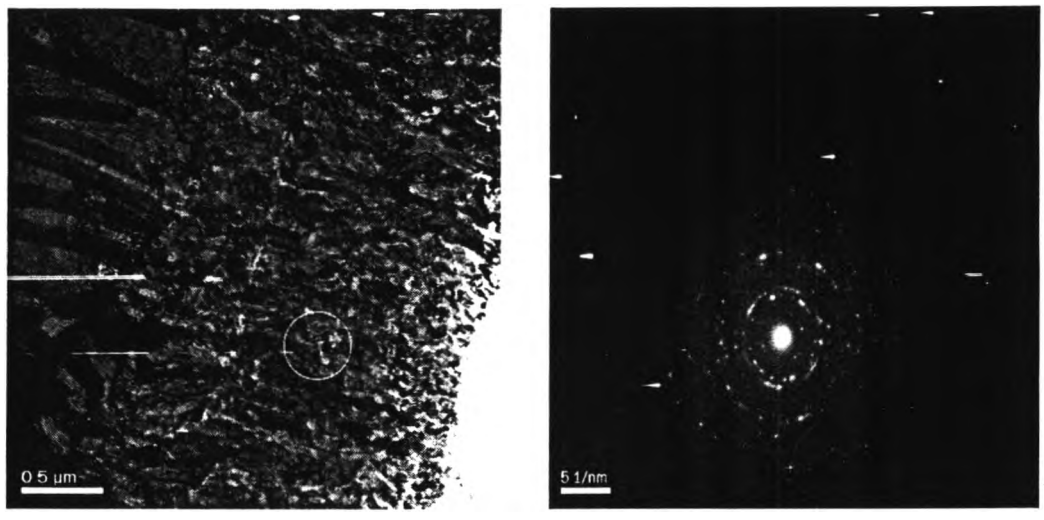

(b) Qinshan_IN_2

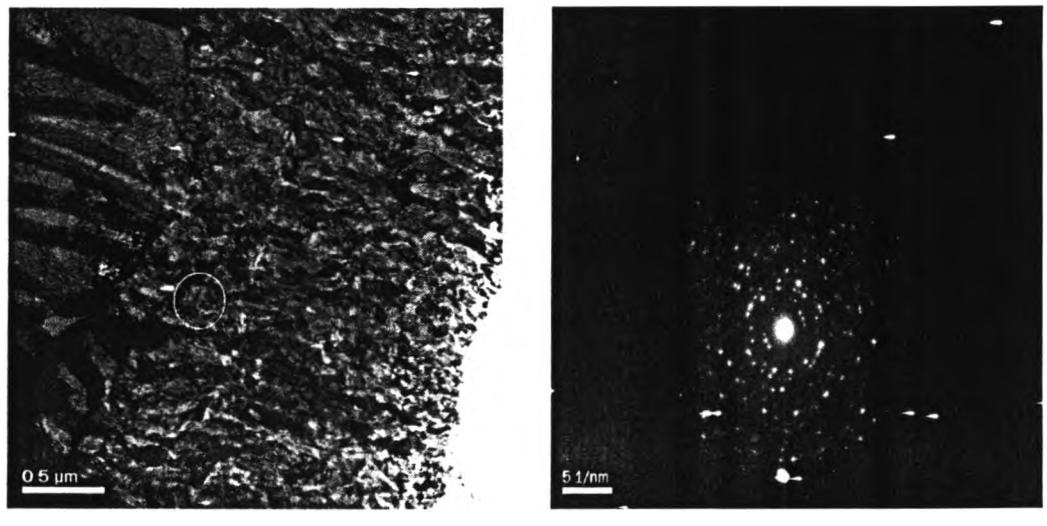

(c) Qinshan_IN_3

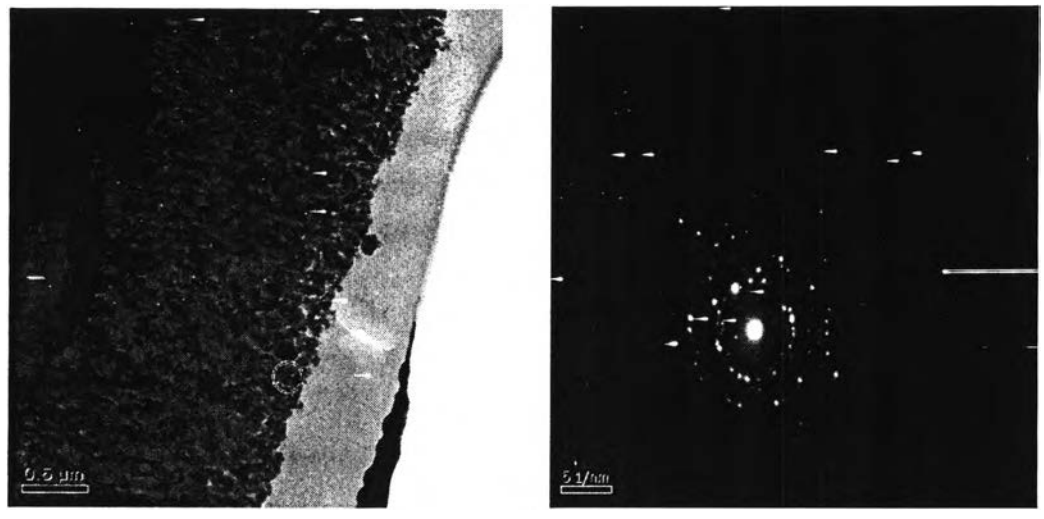

(d) Qinshan_OUT_1

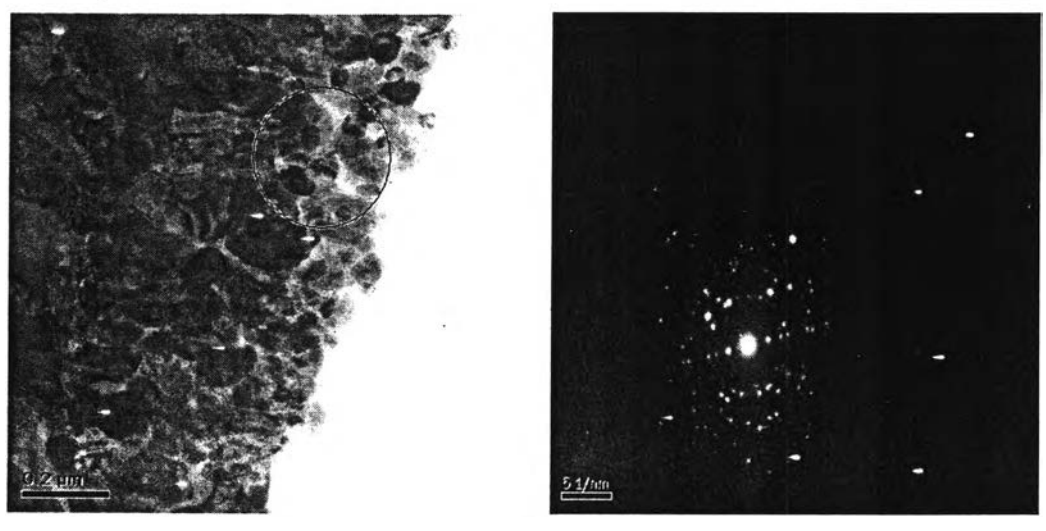

(e) Qinshan_OUT_2

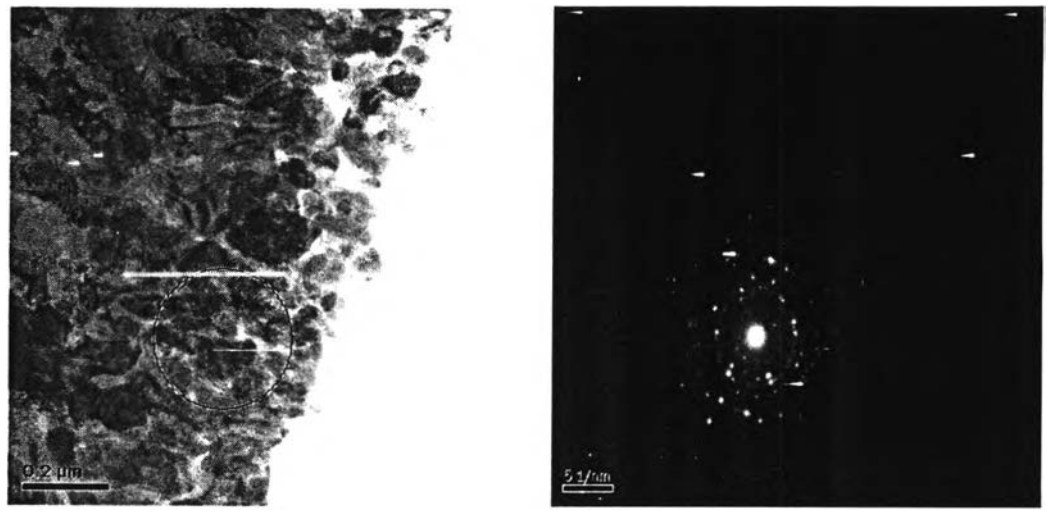

(f) Qinshan_OUT_3

B.3 Electron Diffraction Patterns for 2.5%Cr/1.0%Mo Steel

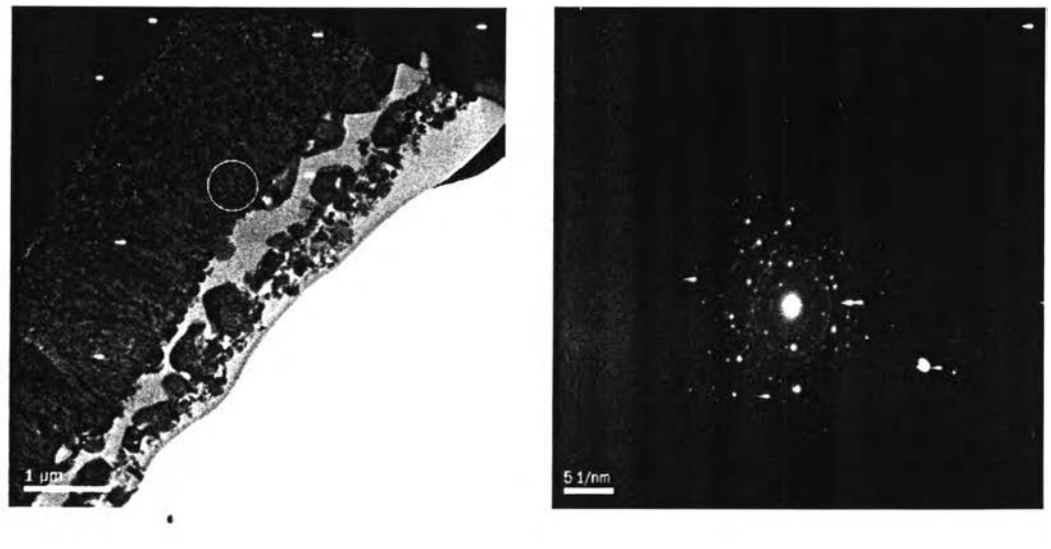

(a) 2.5%Cr_IN_1

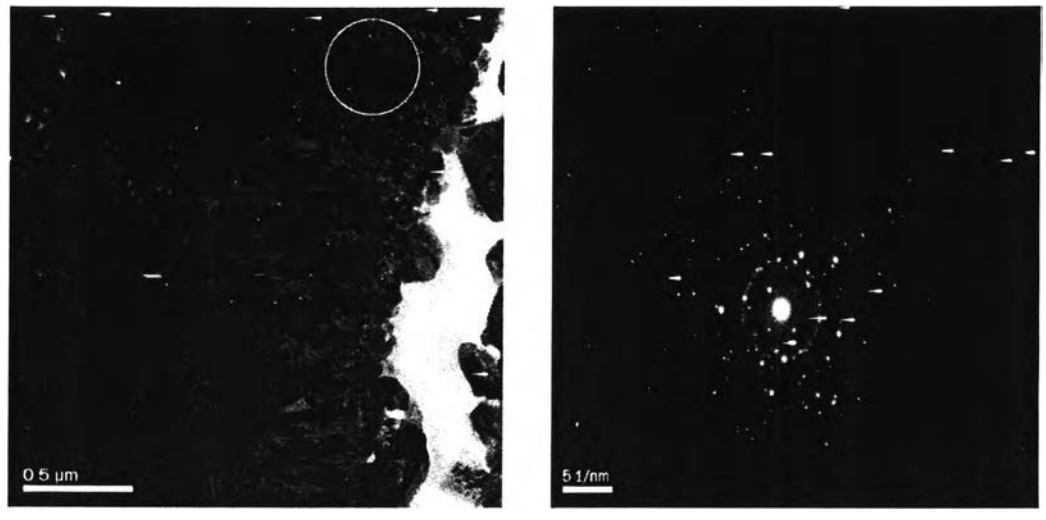

(b) 2.5%Cr_IN_2

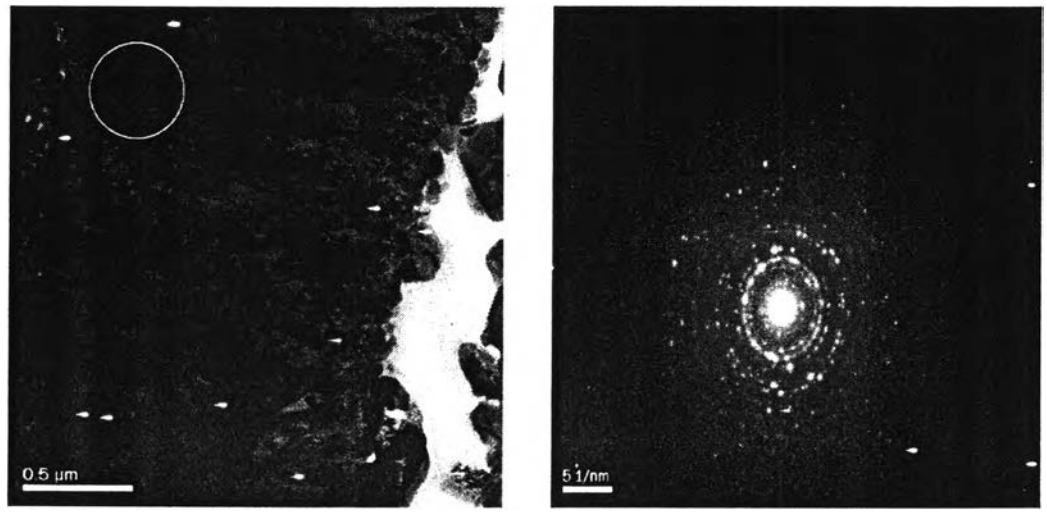

(d) 2.5%Cr_IN_3

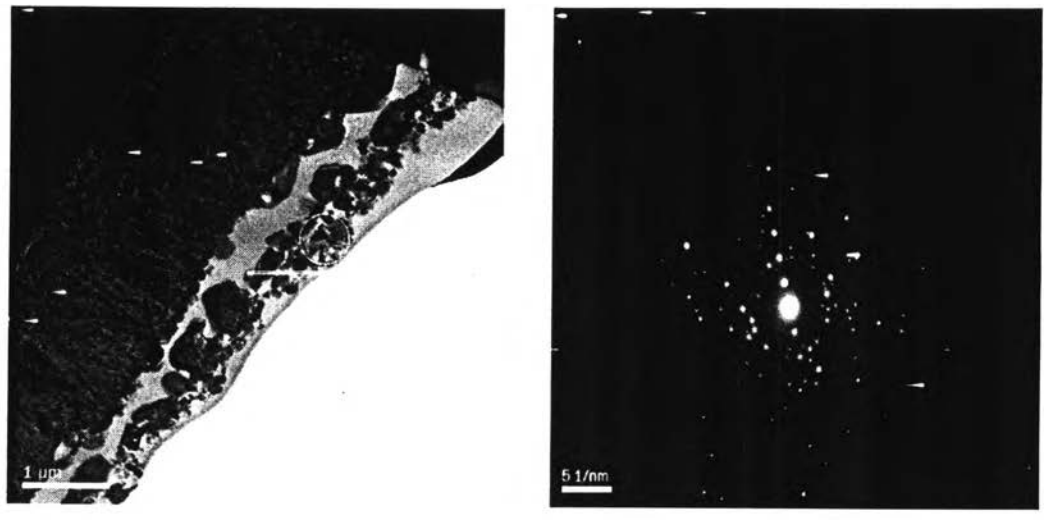

(e) 2.5%Cr_OUT_1

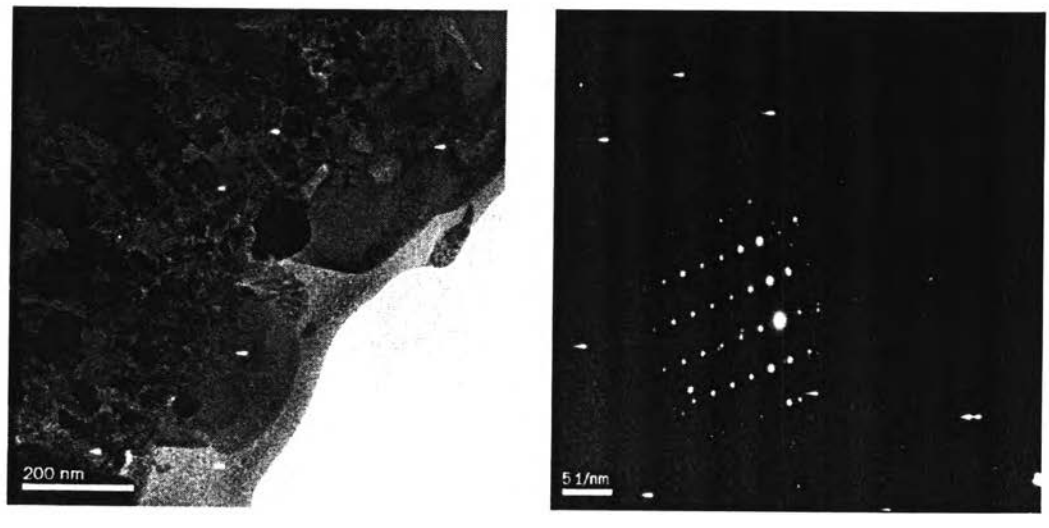

(f) 2.5%Cr_OUT_2

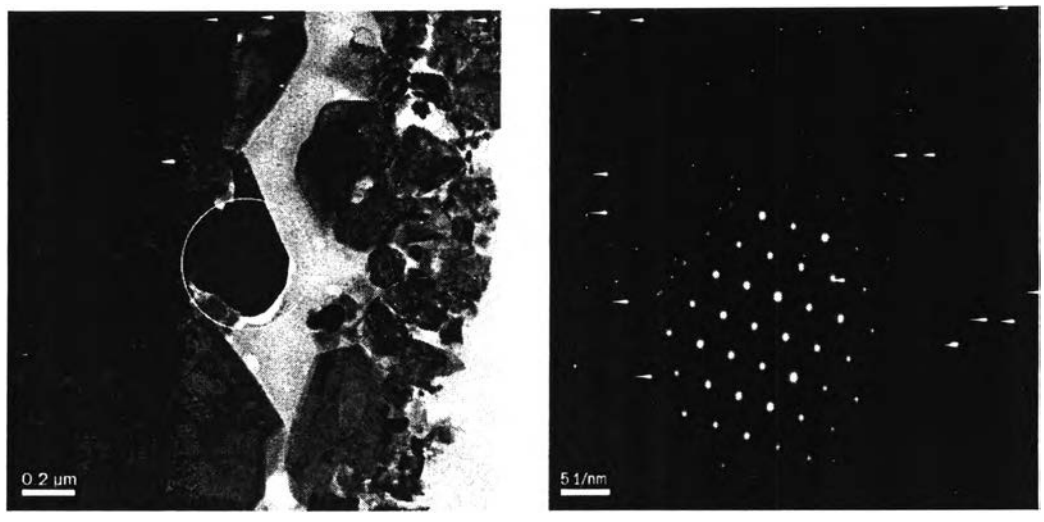

(g) 2.5%Cr_OUT_3

B.4 Electron Diffraction Patterns for 304 Stainless Steel

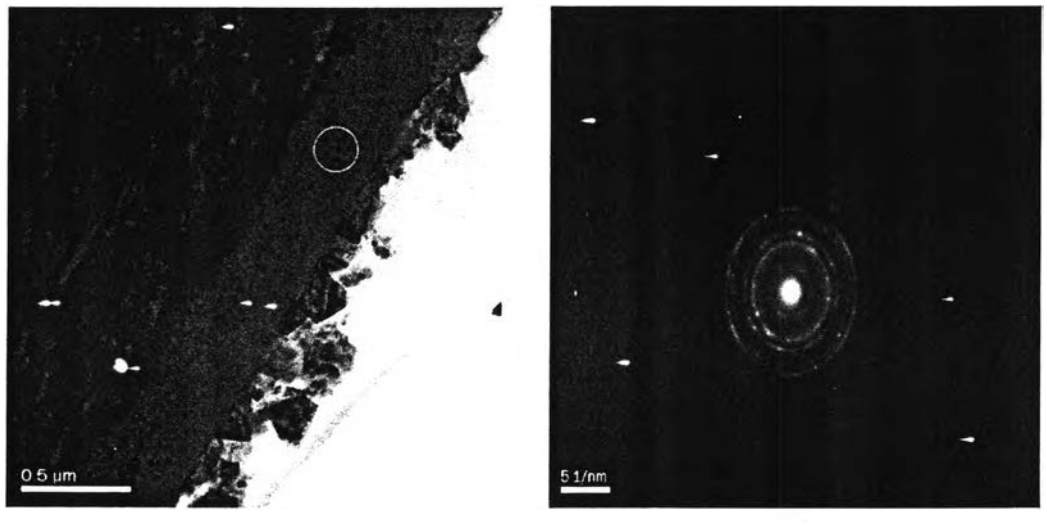

(a) 304SS_IN_1

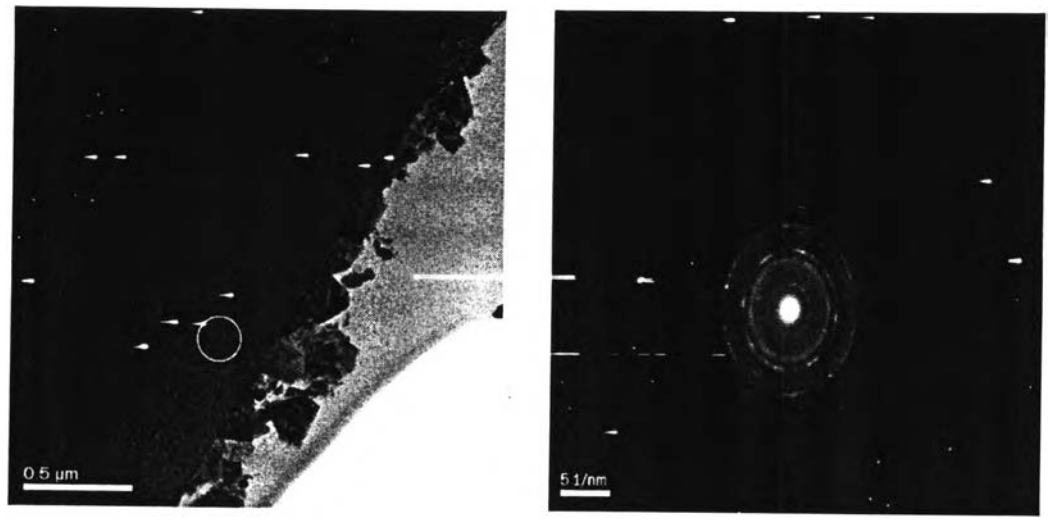

(b) 304SS_IN_2

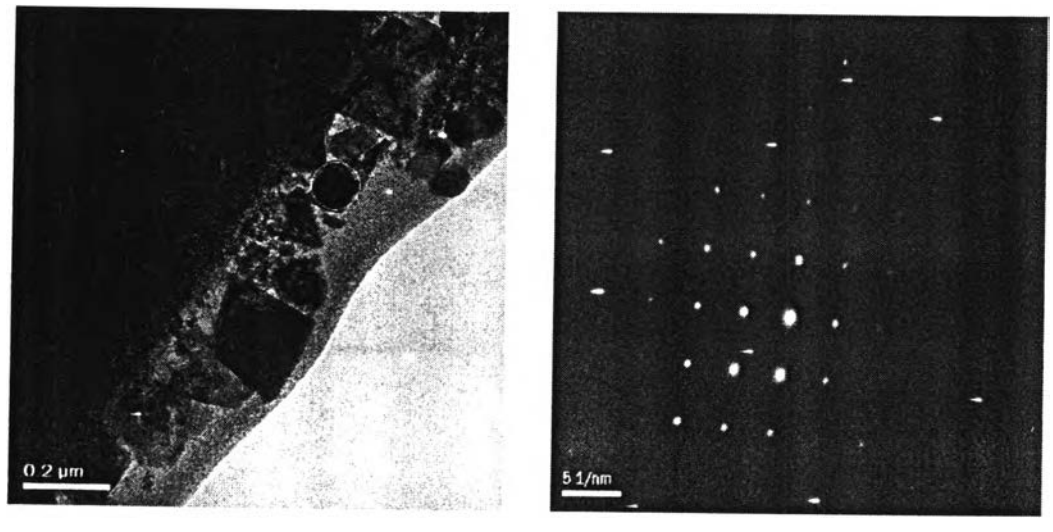

(d) 304SS_OUT_1

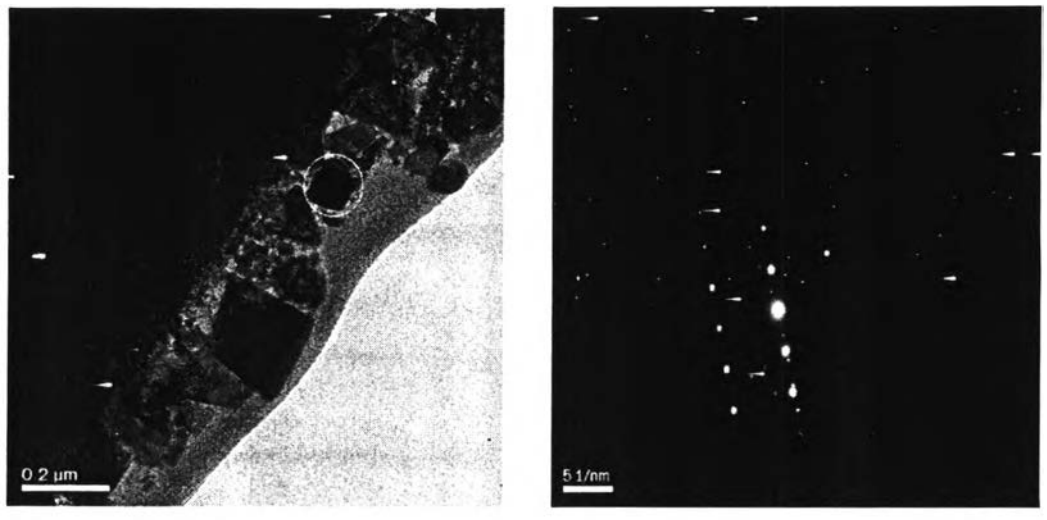

(e) 304SS_OUT_2

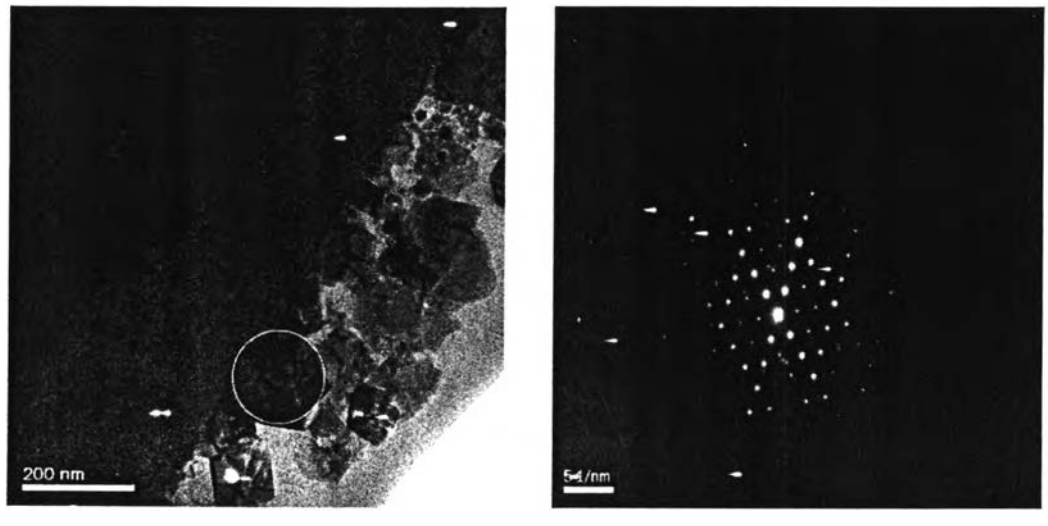

(g) 304SS_OUT_3

Appendix C Lift Out Method

Step 1 Locate the Area of Interest

The location of an area of interest can be done using the FIB microscope's imaging capabilities. Imaging the sample allows the area of interest to be selected visually. For semiconductor devices, the FIB system's precision navigation capabilities can be employed to locate the region of interest with an accuracy that is on the order of microns. The image shows part of a memory array structure of an integrated circuit from which a TEM "lift-out" specimen will be prepared.

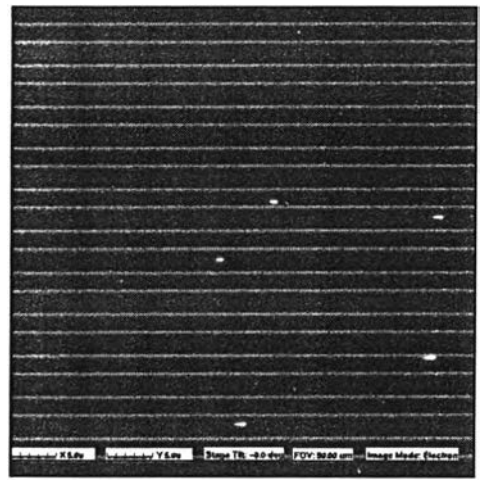

Step 2 FIB-deposit a Protective Tungsten Layer

A layer of FIB-deposited tungsten is placed over the area of interest to prevent milling or multiple image scans from damaging the surface of the TEM specimen cross-section. This step is especially important when surface phenomena on bulk samples are to be analysed. FIB-deposited tungsten provides a fast and precise method for protecting surfaces during FIB procedures.

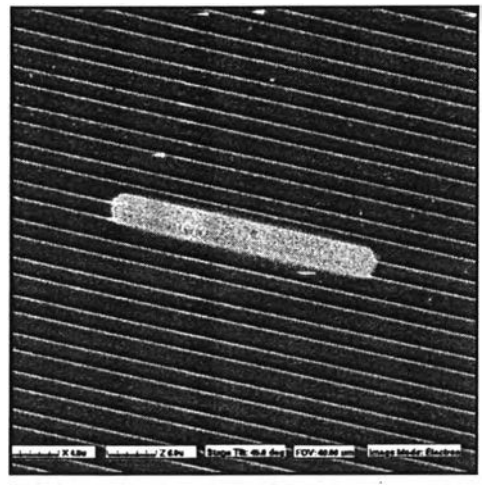

Step 3 Mill Initial Trenches and Rough Polish

Using a large beam current for fast ion milling, two trenches are milled on either side of the tungsten that has been deposited above the area of interest. The trenches here have been milled so as to just touch the tungsten on either side, leaving a wall of material in the centre that is approximately two microns thick. The trenches themselves are approximately twenty microns wide, fourteen microns long and ten to fifteen microns deep.

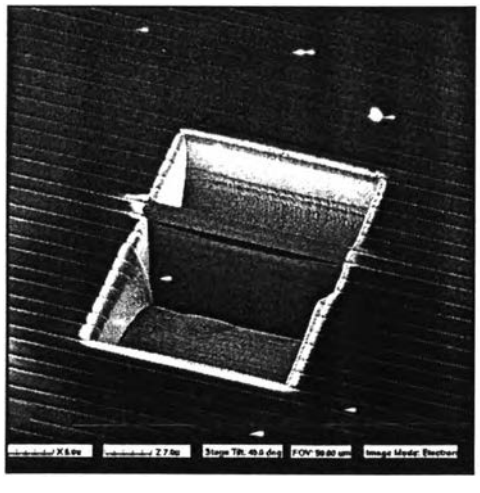

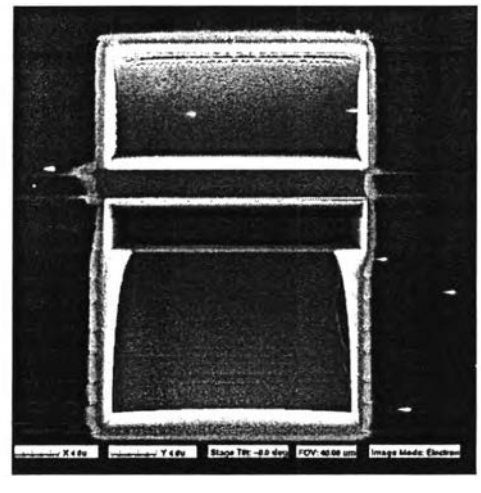

Step 4 Thin the Central Membrane

A smaller beam current is used to further thin the central membrane between the two trenches to a thickness of approximately 1 micrometer. Because milling at a sharp angle, or on an edge, enhances the speed and depth of the mill, the trenches are now stepped, with their deepest points being on either side of the central membrane. One micron is the nominal thickness at which it is recommended to proceed to the next step in the specimen preparation.

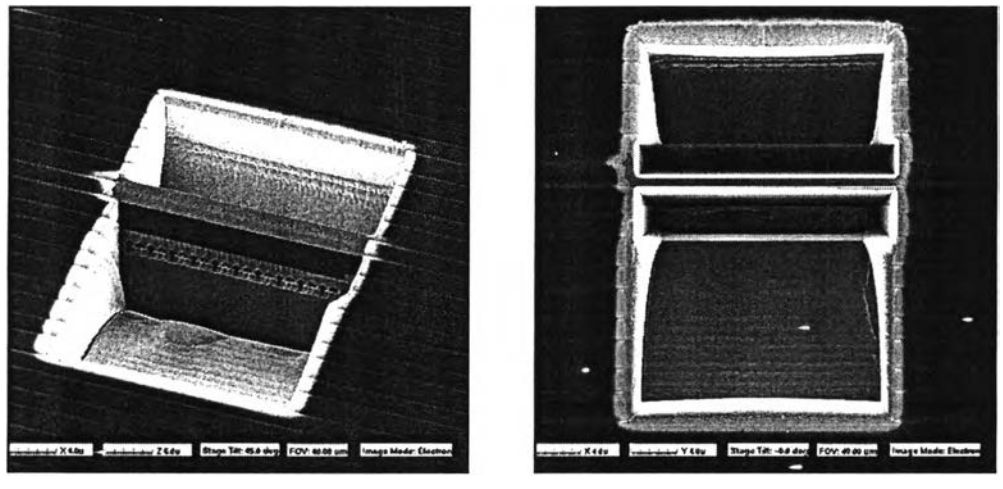

Step 5 Perform "Frame Cuts" on Central Membrane

The bulk sample and the area of interest are tilted to a steep angle, commonly 45° or 60°. Three cuts are made to the central membrane, framing the area of interest. Inside these cuts, the membrane will be ion polished until it is electron transparent. Typically, the membrane is left attached to the bulk at its top two corners. This provides structural strength and stability to the membrane.

Some damage is done to the membrane by tilting and imaging its face. However, since the penetration depth is on the order of nanometers for any given material, any damage done to the cross-section is restricted to essentially the surface of the sample. During the course of the next few steps in the procedure, more than the first two hundred nanometers of material are polished away, ensuring that any

damage to the electron transparent membrane as a result of imaging is not present in the final specimen.

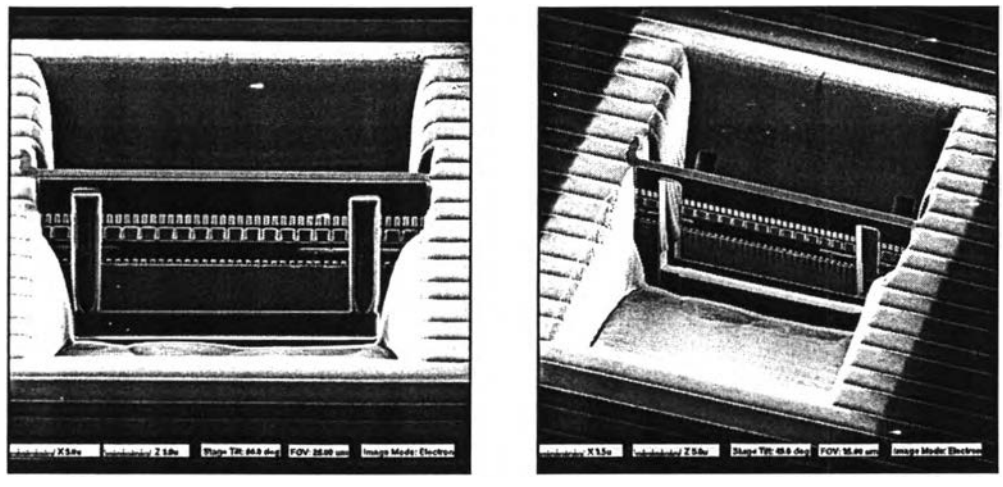

Step 6 "Polish Mills" to Near Nominal Thickness

The beam current is reduced again, and the membrane is ion polished on both sides to a nominal thickness of approximately 0.3 micrometers. At this point, the membrane is very close to being finished. The minimal beam current associated with this step in the procedure leaves the membrane with almost no trace of the ion polish. However, for most materials, 300 nanometers is still much too thick to be electron transparent. So the membrane still requires another very careful, very gentle polishing step.

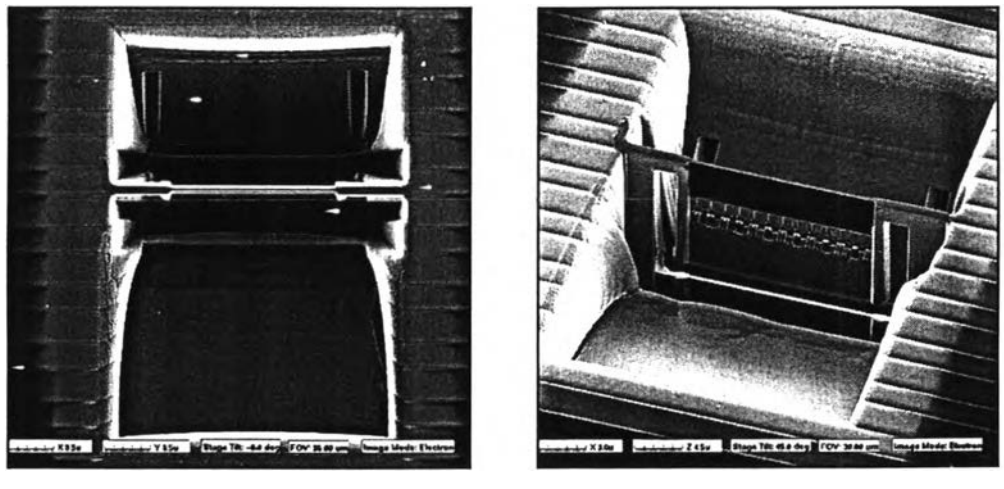

Step 7 Polish for Electron Transparency of Membrane

The last polishing step, again reducing the beam current, brings the membrane to a thickness of between 120 and 50 nanometers. At these thicknesses, the membrane is electron transparent, and will clearly display the cross-section of the area of interest in a TEM. Milling on this nanometer scale demonstrates the precision that FIB microscope-micromachining systems are capable of attaining. This site specificity and precision make FIB systems very useful tools for TEM specimen preparation and any other milling on a microscopic scale.

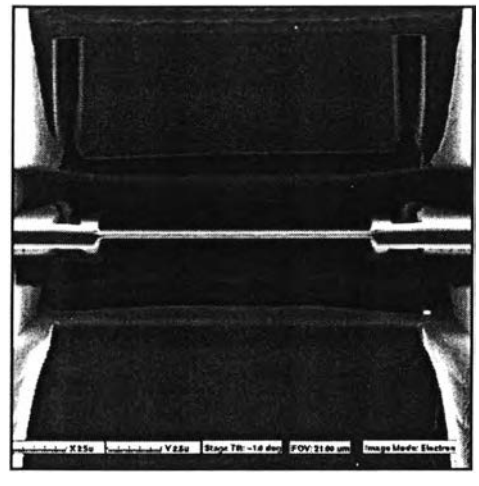

CURRICULIM VITAE

Name: Mr. Teerapong Taenumtrakul

Date of Birth: September 16, 1980

Nationality: Thai

University Education:

1999-2003 Bachelor Degree of Chemical Engineering, Faculty of Engineering, Chulalongkorn University, Bangkok, Thailand

Working Experience:

2002 Position: Student Internship as Process Engineer

Company name: Esso Sriracha Refinery